

---



# SEA: Supervised Embedding Alignment for Token-Level Visual-Textual Integration in MLLMs

---

Yuanyang Yin<sup>1\*</sup>, Yaqi Zhao<sup>2\*</sup>, Yajie Zhang<sup>3</sup>, Ke Lin<sup>3</sup>, Jiahao Wang<sup>3</sup>  
Xin Tao<sup>3</sup>, Pengfei Wan<sup>3</sup>, Di Zhang<sup>3</sup>, Baoqun Yin<sup>1†</sup>, Wentao Zhang<sup>2†</sup>

<sup>1</sup>University of Science and Technology of China

<sup>2</sup>Peking University

<sup>3</sup>Kuaishou Technology

## Abstract

Multimodal Large Language Models (MLLMs) have recently demonstrated remarkable perceptual and reasoning abilities, typically comprising a Vision Encoder, an Adapter, and a Large Language Model (LLM). The adapter serves as the critical bridge between the visual and language components. However, training adapters with image-level supervision often results in significant misalignment, undermining the LLMs' capabilities and limiting the potential of Multimodal LLMs. To address this, we introduce Supervised Embedding Alignment (SEA), a token-level alignment method that leverages vision-language pre-trained models, such as CLIP, to align visual tokens with the LLM's embedding space through contrastive learning. This approach ensures a more coherent integration of visual and language representations, enhancing the performance and interpretability of multimodal LLMs while preserving their inherent capabilities. Extensive experiments show that SEA effectively improves MLLMs, particularly for smaller models, without adding extra data or inference computation. SEA also lays the groundwork for developing more general and adaptable solutions to enhance multimodal systems.

## 1 Introduction

Multimodal Large Language Models (MLLMs) rapidly developed in recent years, showing impressive abilities in multimodal perception and reasoning [2, 5, 33]. These models bridge the gap between different modalities, enabling more comprehensive and context-aware interactions. The evolution of MLLMs represent a significant advancement in artificial general intelligence (AGI), as it mimics how humans interact with the world and comprehend complex information through different senses.

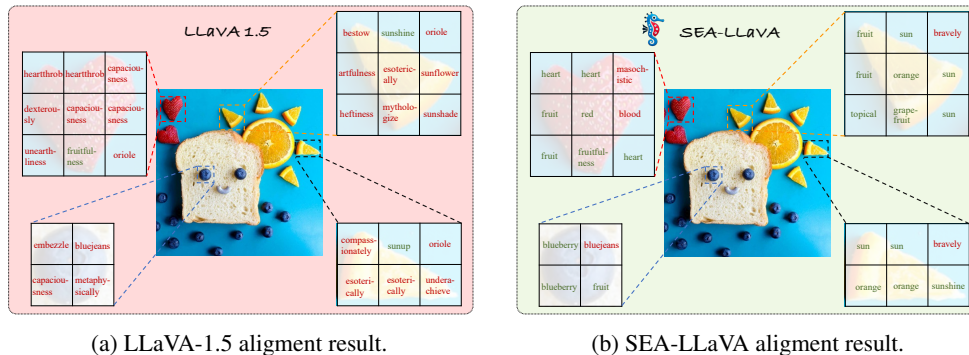
Traditional training paradigms in MLLMs typically involve two key phases: pre-training and instruction-tuning [14, 22, 33, 34, 52]. During the pre-training phase, the adapter is solely trained to enhance its ability to transform visual representations into text, thereby understanding the relevance of image contents and their corresponding textual descriptions, and facilitating effective cross-modal alignment. The instruction-tuning phase further enhances the model's adaptability to specific tasks.

However, this pre-training paradigms face inherent limitations due to the mismatch between the frozen language model, trained primarily on text tokens, and the visual features, which often lack direct textual equivalents. Moreover, the training approach primarily involves simple and implicit supervision, where losses are computed only for predicting language responses. In this setup, visual information acts merely as contextual cues without serving as direct supervision for alignment with

---

\* Equal Contribution.

† Corresponding Author.



(a) LLaVA-1.5 alignment result.

(b) SEA-LLaVA alignment result.

**Figure 1: Comparison of Alignment Results between LLaVA-1.5 and SEA-LLaVA.** After 2 stages of training, we evaluate the alignment of visual tokens with the LLM’s embedding space by measuring the similarity between visual tokens and the words encoded by the LLM. The word with the highest semantic relevance to each visual token is selected as its representation. Correct alignments are marked in green, while incorrect ones are in red. SEA-LLaVA, which is an improved version of LLaVA-1.5 without introducing new data, shows significantly better alignment.

textual representations. In this paper, we will show that this paradigm cannot effectively guide the adapter in achieving accurate alignment between visual and textual features, a phenomenon we refer to as misalignment (See Figure 1), leading to inconsistencies in the model’s understanding and generation capabilities(See Figure 2). This issue is exacerbated during instruction-tuning, where the entire LLM must be fine-tuned. Poor initialization from the pre-training phase results in suboptimal adapter weights, making the fine-tuning process more challenging and potentially degrading both the model’s language capabilities and overall multimodal performance.

Several recent works have sought to improve alignment in MLLMs. For example, [39] uses an optimal transport-based method to align pre-trained vision model embeddings with the LLM’s space, though it is limited by its reliance on image-caption pairs and is specific to encoder-decoder models. Similarly, [42] maps visual features to LLM vocabulary through regression, but it struggles with precise token-level alignment. Additionally, [47] enhances alignment by annotating images with alphanumeric tags, improving object-text alignment but requiring extensive data annotation and adding complexity. These methods still face challenges with misalignment, leading to information loss and hindering the LLM’s understanding of visual content.

In this work, we address a critical issue: *How to resolve insufficient alignment in MLLMs?* To tackle this, we propose a novel token-level supervised alignment paradigm called Supervised Embedding Alignment (SEA). SEA uses explicit supervision to precisely align visual tokens with the LLM’s embedding space. Unlike traditional image-level methods, our approach ensures that each visual token is precisely matched with its corresponding semantic representation within the LLM, following the trend of treating visual and textual tokens as equivalent inputs. Specifically, SEA improves alignment in mainstream MLLMs through two key aspects.

**Token-Level Labeling for Fine-Grained Alignment.** During the pre-training stage, a captioning task trains an adapter to align visual patches with the LLM’s embedding space, enabling visual tokens to be treated like text tokens. However, current image-level alignment methods are coarse and lack fine-grained guidance, leading to suboptimal results. There are two main challenges impede achieving token-level fine-grained alignment. First, since a visual token’s semantic representation is continuous, a single visual token often encapsulates multiple meanings. No current models can generate multiple semantic labels for each visual token, making it impossible to provide fine-grained alignment guidance. Second, visual encoders often produce semantic shifts, where a token’s representation reflects surrounding image regions, complicating the accurate mapping of visual patches to their corresponding semantic labels. Existing methods highlight the suitability of vision encoders for MLLMs but often overlook the value of text encoders (paired with vision encoders during training). Since visual representations from the vision encoder align naturally with text representations, we use the text encoder to infer semantic labels for each visual token. This approach addresses the continuous semantic token-level labeling challenge and mitigates semantic shifts, enabling effective token-level alignment.

**A Novel Supervised Alignment Paradigm.** Mainstream approaches that apply image-level supervision at the LLM’s outputs diverge from the goal of treating visual and textual tokens equally, making it difficult to bridge the gap between them. To address this, we propose a novel alignment supervision paradigm that directly aligns visual tokens with textual tokens, enabling the LLM to process visual tokens in a manner similar to textual tokens. Specifically, by leveraging semantic labels for each visual token and employing contrastive learning, we ensure that visual token representations closely match their corresponding semantic labels in the LLM’s embedding space. By combining contrastive learning loss with LLM prediction loss to update the adapter, we effectively enhance its alignment capability, bridging the gap between the vision encoder and the LLM.

Leveraging our proposed SEA, we have significantly enhanced the performance of the LLaVA-1.5 across 8 benchmarks, without needing extra annotations, data, or inference costs. This method offers a universal, cost-effective training strategy for vision encoders trained on vision-language tasks, showcasing high returns and exceptional innovation.

## 2 Related Work

**Vision-Language Pre-Training.** The integration of computer vision and natural language processing has resulted in Vision Language Models (VLMs). These models combine visual and linguistic components, typically leveraging image-text pairs, to enrich visual information with semantic content and facilitate cross-modal understanding. Contrastive learning has become particularly influential in the realm of Vision-Language pre-training since the introduction of models like CLIP [40], ALIGN [21], SPARC [8]. These methods utilize softmax contrastive learning on large-scale image-text datasets. Unlike above methods that require a global view of pairwise similarities for normalization, SigLIP [49] proposes a simple approach with a pairwise Sigmoid loss that operates solely on image-text pairs. These models have demonstrated exceptional zero-shot transfer capabilities, leading to enhanced performance in tasks that require comprehensive understanding of both modalities.

**Cross-Modal Alignment in MLLMs.** The combination of image and text representations is essential for MLLMs, which can be categorized into two main types based on their fusion approach: *deep fusion* and *shallow fusion*. In *deep fusion* [4, 6, 26, 46], image features encoded by the vision encoder are integrated into the language model layers via interaction modules, allowing text to attend to image features. Conversely, *shallow fusion* [15, 24, 27, 34, 52] concatenate the vision encoder’s output directly with text embeddings before passing them to the language model. These methods show that vision models and LLMs, though independently trained, share significant information. However, there are concerns that shallow fusion approaches fail to fully bridge the gap between visual and language model representations, limiting the LLM’s comprehension of visual tokens. To address this, [50] proposes assigning a special token to different image-text pairs based on similarity scores. This asymmetrical learning approach enhances the adapter’s alignment capability, improving the language model’s understanding of visual tokens. [32] enhances visual tokens by reintroducing information extracted from segmentation and OCR models back into the visual tokens. While these approaches have achieved significant breakthroughs, they fall short of fundamentally enhancing the adapter’s alignment capability. This paper introduces SEA (Supervised Embedding Alignment) as a more effective solution to improve this alignment.

## 3 Preliminaries

In this section, we first introduce the typical adapter module that bridges the vision encoder and LLM in MLLMs. Following this, we highlight the issue of misalignment and its impacts, forming the basis for our method presented in Section 4.

**Adapter in Multimodal LLMs.** Multimodal Large Language Models aim to integrate visual and textual information seamlessly. A common approach involves using an adapter, typically positioned between the vision encoder and a large language model. The adapter can be a simple linear layer [34] or a more complex multi-layer perceptron [33]. For clarity, we define the visual features output by the vision encoder as *visual patches* and the features after passing through the adapter as *visual tokens*. During pre-training, this module transforms visual patches into representations compatible

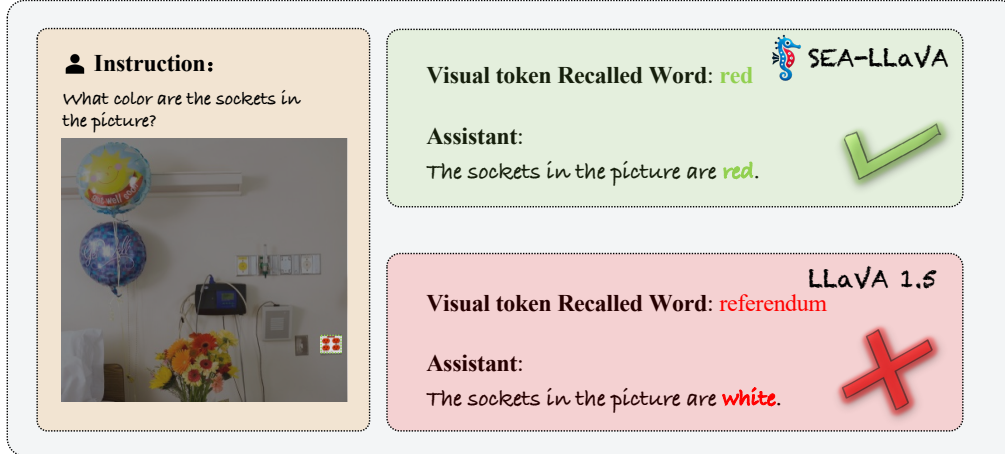


Figure 2: **Impact of Visual Token Alignment on Model Performance.** The "recalled word" refers to the word with the highest similarity score for a given visual token. In this example, we asked a question about the visual elements in the dashed green box. LLaVA-1.5 failed to answer correctly due to misalignment of the visual token, selecting "referendum" instead of a relevant color. In contrast, SEA-LLaVA correctly aligned the visual token to the LLM's embedding space, resulting in the correct response "red."

with the LLM's textual representations. The goal is to refine these visual tokens to closely match their semantic information in the LLM's embedding space.

During the pre-training, for a given image-text pair  $(X_{\text{image}}, X_{\text{text}})$ . The LLM input is constructed as:

$$X_v = g_{\theta}(f(X_{\text{image}})) \quad (1)$$

$$X_t = \Psi(X_{\text{text}}) \quad (2)$$

$$X_{\text{input}} = [x_{v_0}, \dots, x_{v_m}, x_{t_0}, \dots, x_{t_n}], \quad x_{v_j} \in X_v \quad x_{t_i} \in X_t \quad (3)$$

where  $f$  represents for vision encoder,  $g$  represents for the adapter, and  $\Psi$  is LLM's embedding layer. Subsequently,  $X_{\text{input}}$  is passed to the LLM for generating the response, and the parameter  $\theta$  of the  $g$  is updated by calculating the auto-regressive loss.

**Misalignment Issue.** Despite the pre-training efforts to align visual tokens with text tokens in the LLM's embedding space, current models exhibit significant misalignment issues. The adapter, which is implicitly supervised through auto-regressive loss, fails to ensure accurate semantic representations of each visual patch during pre-training. As a result, a notable discrepancy arises between visual and textual tokens in the LLM's embedding space after 2 stages of training as shown in Figure 1.

**Impacts of Misalignment.** The misalignment after pre-training leads to significant information loss, profoundly affecting the MLLMs' comprehension and performance. When the language model cannot comprehend the misaligned tokens, it leads to incorrect responses and severe hallucinations, as depicted in Figure 2. Furthermore, if the language model is unfrozen during fine-tuning, the divergence between visual and textual representations is exacerbated, increasing the difficulty of training and severely damaging the LLM's language capabilities.

To investigate these concerns, we removed the pre-training stage and directly fine-tuned the model. This approach led to a significant performance drop across multiple benchmarks, including pure language tasks (See Figure 3). The "Vicuna-7B" baseline scored 47.1, while the "LLaVA w/o pretrain" model, directly fine-tuned without pre-training, dropped to 38.9, showing a 17% performance decrease due to the interference from unaligned visual tokens, leading to catastrophic forgetting. When pre-training is included, the adapter aligns the visual tokens with the LLM's embedding space, preventing significant degradation during fine-tuning. Despite the alignment effect achieved during pre-training, the language model's capabilities are still substantially impaired, indicating that cross-modality alignment remains a challenging task. Notably, our proposed SEA scored 46.4, demonstrating

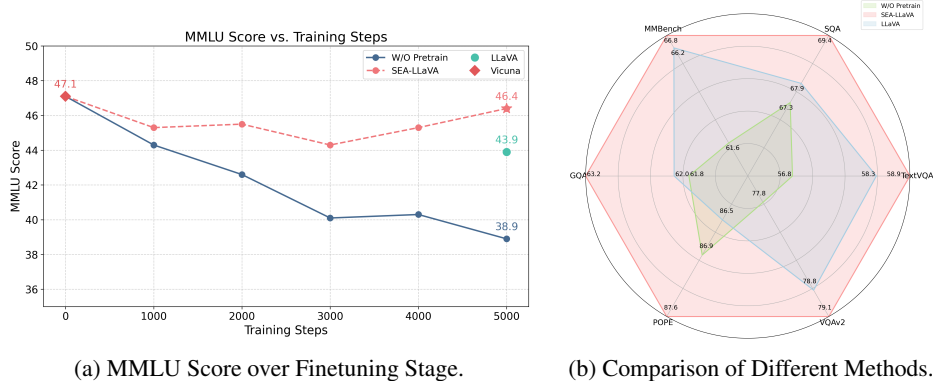


Figure 3: (a) The impact of removing the pre-training stage on MMLU scores during the fine-tuning phase. The performance exhibits a significant decline when pre-training is omitted, highlighting its crucial role. In contrast, the SEA-LLaVA method (red line) maintains almost the same initial language capabilities throughout the fine-tuning process, demonstrating its robustness. (b) A comparative analysis of different methods across various benchmarks illustrates the effectiveness of the SEA-LLaVA method in maintaining superior performance.

that our method effectively preserves language capabilities during fine-tuning and maintains robust performance across multimodal tasks.

We propose a novel token-level supervision alignment paradigm during pre-training to address the misalignment of visual and text tokens in the LLM’s embedding space. This aims to mitigate information loss and improve the overall representation of both modalities.

## 4 Supervised Embedding Alignment: Method

This section presents SEA, the first supervision paradigm to mitigate the issue of misalignment between visual and text tokens in LLM’s embedding space during pre-training (See Figure 4). SEA leverages the rich visual features extracted from vision-language pre-trained models, which are already well-aligned with the text encoder’s space. As shown in the Figure 5, for each patch in the image, SEA first utilizes the vision-language pre-trained model to select words that can maximize the cosine similarity between visual and text features from a pre-defined list, which serves as the label for each patch in the image. Subsequently, it guides the alignment between visual tokens and text tokens in the LLM’s embedding space through contrastive learning during pre-training. We will introduce each step of SEA in detail below.

### 4.1 Extract Semantic Labels for Visual Patches

To achieve fine-grained supervision of the semantic feature expression of each visual token transformed by the adapter, we need to obtain the continuous semantic labels of each patch after the vision encoder. For a vision-language pre-trained vision encoder  $f$  paired with a corresponding text encoder  $h$  and a word list  $W$ , we extract the semantic information for each patch using Eqs. (4), (5), (6). We then select the top  $n$  words based on their cosine similarity scores for each visual patch (See Figure 5(3)). To ensure only the most relevant and positively correlated words are considered, we exclude any labels with similarity scores less than 0. The remaining words are referred to as the *semantic labels* for each visual patch. This approach assigns multiple semantic labels to each token, preserving the continuous semantic representation of the aligned visual token. Paired training of the vision and text encoders also effectively prevents semantic shift.

$$V = f(X_{\text{image}}) \in \mathcal{R}^{m \times d} \quad (4)$$

$$T = h(W) \in \mathcal{R}^{q \times d} \quad (5)$$

$$w_i, s_i = \underset{j}{\operatorname{argmax}} \{-\cos(v_i, t_j)\} \quad (6)$$

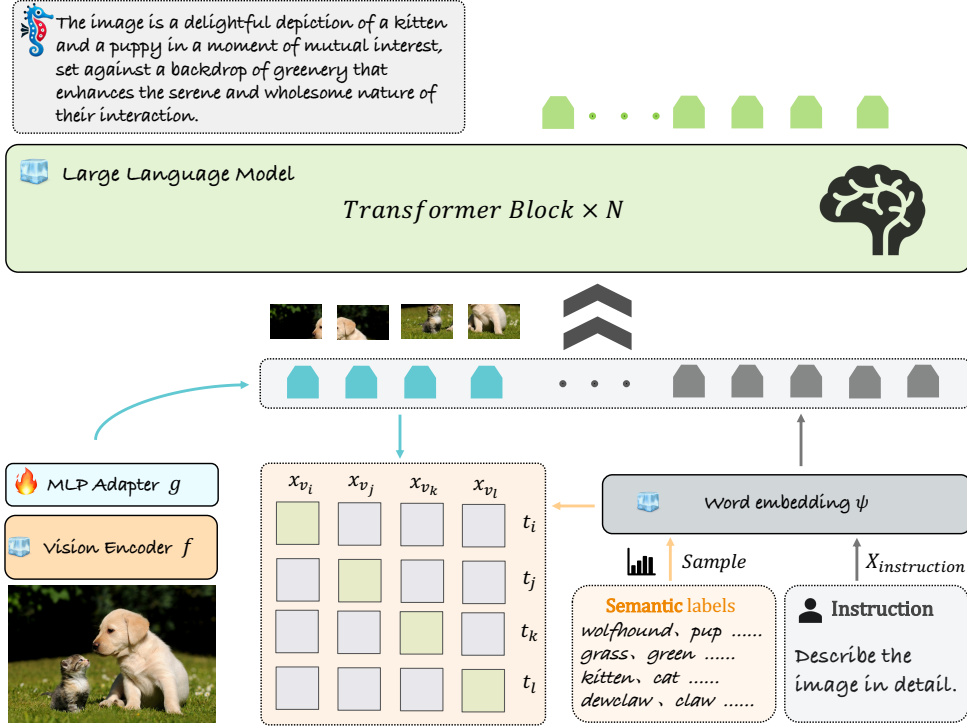


Figure 4: **Overview of the proposed SEA.** During pre-training, LLM’s embedding layer encodes both instructions and semantic labels simultaneously. These encoded semantic labels directly guide the alignment of visual tokens to the LLM’s embedding space through contrastive learning. The visual tokens are then concatenated with the instructions and input into the LLM to generate a response.

where  $w_i$  and  $s_i$  are the indices and scores of the top  $n$  semantic labels for the  $i$ -th visual patch  $v_i$  respectively.  $v_i$  is the visual feature of the patch obtained from the vision encoder  $f$ , and  $t_j$  is the text embedding of the  $j$ -th word in the word list  $W$ , obtained from the text encoder  $h$ . The negative cosine similarity  $-\cos(v_i, t_j)$  is computed as described in previous works [30], where the cosine similarity needs to be negated in the CLIP embedding space.

## 4.2 Token-Level Alignment

The use of an adapter aims to convert visual patches into LLM’s embedding space. However, the current image-level approach falls short of achieving this adequately as shown in Figure 1a. We suggest using the semantic labels of each patch to directly guide the adapter in transforming visual patches into the LLM’s embedding space, thereby reducing misalignment (See Figure 1b).

**Similarity-Weighted Sampling for Continuous Semantic Representation.** Due to the semantic continuity of visual tokens, we should identify an appropriate position for each visual token within the LLM’s embedding space, ensuring it retains its continuous semantic representation. Specifically, for a given visual patch  $v_i$  with its corresponding semantic labels  $L_i = [w_1, \dots, w_n]$  and similarity scores  $S_i = [s_1, \dots, s_n]$ , we first normalize the similarity scores to get the sampling probability, and then sample a label for each patch based on  $S_{norm}^i$  in Eq. (7).

$$S_{norm}^i = \frac{S_i}{\text{sum}(S_i)} \quad (7)$$

**A Localized Sampling Strategy.** To further enhance the effectiveness of contrastive learning and mitigate the issue of excessive similarity between samples, we adopt a localized sampling strategy. For each image, we perform sampling within a  $k \times k$  window, ensuring that only one patch is sampled from each window. Consequently, a single image with  $N$  visual patches will have  $N/(k \times k)$  patches



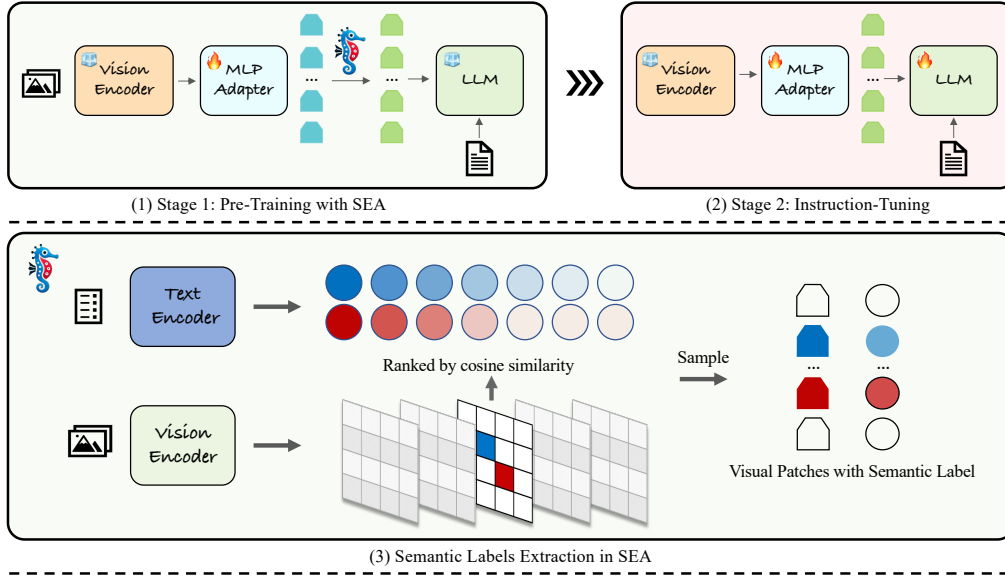


Figure 5: **Overview of the SEA training pipeline.** (1) Pre-Training with SEA. This stage uses the SEA to enhance modality alignment between vision and language models. Only the adapter is optimized. (2) Instruction-Tuning. Both the LLM and the adapter are fine-tuned, ensuring improved multimodal performance. (3) Illustration of Semantic Label Extraction for SEA. During pre-training, semantic labels for visual patches are extracted from a word list using vision-language pre-trained models. Circular shapes represent candidate labels, and irregular hexagons represent visual patches. These labels are ranked by cosine similarity, and then sampled according to their similarity-weighted ranking to provide explicit supervision and enhance modality alignment.

participating in contrastive learning. For visual patches sharing the same label in one batch, we randomly retain only one patch to ensure the effectiveness of contrastive learning. We then obtain a series of visual patches with labels, namely,  $\{(x_{v_1}, w_1), \dots, (x_{v_N}, w_N)\}$ , where  $N$  is the number of tokens in one batch.

For each label  $w_i$ , we compute the corresponding text feature  $t_i$  as follows:

$$t_i = \frac{1}{M} \sum_{k=1}^M \Psi(w_i^k) \quad (8)$$

where  $\Psi(w_i^k)$  represents the encoded feature of the  $k$ -th token of  $w_i$ , and  $M$  is the number of tokens after encoding  $w_i$ .

The loss of alignment can be computed as:

$$\mathcal{L}_a = -\frac{1}{2N} \sum_{i=1}^N \left( \log \frac{\exp(\phi(\mathbf{x}_{v_i}, \mathbf{t}_i)/\tau)}{\sum_{j=1}^N \exp(\phi(\mathbf{x}_{v_i}, \mathbf{t}_j)/\tau)} + \log \frac{\exp(\phi(\mathbf{t}_i, \mathbf{x}_{v_i})/\tau)}{\sum_{j=1}^N \exp(\phi(\mathbf{t}_i, \mathbf{x}_{v_j})/\tau)} \right) \quad (9)$$

where  $\phi(\mathbf{x}_{v_i}, \mathbf{t}_j) = \frac{\mathbf{x}_{v_i} \cdot \mathbf{t}_j}{\|\mathbf{x}_{v_i}\|_2 \cdot \|\mathbf{t}_j\|_2}$ , and  $\tau$  is the temperature, a learnable parameter.

For generation, the prediction of the next token  $x^{(i)}$  is conducted based on visual tokens  $V_i$ , prompt  $P$  and previous tokens  $x^{(<i)}$ . The loss can be computed as:

$$\mathcal{L}_g = -\frac{1}{B} \sum_{i=1}^B \log p_\theta \left( x^{(i)} \mid V_i, P, x^{(<i)} \right) \quad (10)$$

where  $B$  is the batch size,  $\theta$  is the trainable parameters.

During the pre-training process, two learning objectives simultaneously supervise the adapter. We obtain the final loss  $\mathcal{L}$  of pre-training by adding  $\mathcal{L}_a$  and  $\mathcal{L}_g$ , a weighting factor  $\lambda$  is introduced to

balance the two losses.

$$\mathcal{L} = \mathcal{L}_g + \lambda \mathcal{L}_a \tag{11}$$

## 5 Experiments

In this section, we first provide our experimental framework and evaluation results on 8 common benchmarks compared with different backbones in Table 1. Subsequently, we empirically investigate the effectiveness and robustness of SEA.

**Table 1: Main evaluation results compared with leading baselines on 8 popular benchmarks.** VQA<sup>v2</sup> [17]; VQA<sup>T</sup>: TextVQA [44]; GQA [20]; SQA<sup>I</sup>: ScienceQA-IMG [36]; MMB: MMBench [35]; POPE [28]; VizWiz [18]; MM-Vet [48]. SEA-PRIME outperforms other open-source models and achieves competitive performance. All methods maintain the number of visual tokens without doubling, and models marked with \* are results we reproduced. Column Res. is the image resolution of vision model.

Method	LLM	Res.	VQA <sup>v2</sup>	VQA <sup>T</sup>	GQA	SQA <sup>I</sup>	MMB	POPE	VizWiz	MM-Vet
MobileVLM-3B[12]	MLLaMA 2.7B	336	–	47.5	59.0	61.0	59.6	84.9	–	–
MobileVLM-V2-3B[13]	MLLaMA 2.7B	336	–	57.5	61.1	70.0	63.2	84.7	–	–
LLaVA-Phi [53]	Phi-2.7B	336	71.4	48.6	–	68.4	59.8	85.0	35.9	28.7
TinyLLaVA [51]	Phi-2.7B	384	79.9	59.1	62.0	69.1	66.9	86.4	–	32.0
InstructBLIP [14]	Vicuna-7B	224	–	50.1	–	–	30.6	–	34.5	–
InstructBLIP [14]	Vicuna-13B	224	–	50.7	49.5	63.1	–	–	33.4	–
Qwen-VL [7]	Qwen-7B	448	79.5	63.8	59.3	67.1	38.2	–	35.2	–
Qwen-VL-Chat [7]	Qwen-7B	448	78.2	61.5	57.5	68.2	60.6	–	38.9	–
LLaMA-VID [29]	Vicuna-7B	336	79.3	–	64.3	68.3	65.1	86.0	54.2	–
LLaMA-VID [29]	Vicuna-13B	336	80.0	–	65.0	70.0	66.6	86.0	54.3	–
LLaVA-1.5* [33]	Vicuna-7B	336	78.8	58.3	62.0	67.9	66.2	86.5	45.7	30.7
LLaVA-1.5* [33]	Vicuna-13B	336	80.0	60.8	63.3	71.6	67.7	87.6	53.6	35.1
ShareGPT4V [9]	Vicuna-7B	336	80.6	–	–	68.4	68.8	–	–	37.6
Mini-Gemini [31]	Gemma-2B	336+768	–	56.2	–	–	59.8	–	–	31.1
Mini-Gemini [31]	Vicuna-7B	336+768	–	65.2	–	–	69.3	–	–	40.8
Mini-Gemini [31]	Vicuna-13B	336+768	–	65.9	–	–	68.5	–	–	46.0
S <sup>2</sup> -Wrapper* [43]	Vicuna-7B	1008	79.7	60.3	63.2	–	67.3	87.4	50.1	33.0
S <sup>2</sup> -Wrapper [43]	Vicuna-13B	1008	80.9	63.1	–	–	67.9	–	56.0	35.4
AlignGPT [50]	Vicuna-7B	336	79.1	58.4	62.9	68.5	67.3	86.0	54.2	30.8
AlignGPT [50]	Vicuna-13B	336	80.0	60.2	63.6	70.3	69.5	86.2	56.4	35.6
Visual Prompt [32]	Vicuna-7B	336	79.8	59.8	63.3	69.5	67.6	<b>88.9</b>	–	34.9
<i>Our Models</i>										
<b>SEA-PRIME</b>	Gemma-2B	384	81.0	60.7	62.4	69.2	68.8	87.8	61.9	38.0
<b>SEA-PRIME</b>	Phi3-3.8B	384	80.7	64.0	62.0	78.7	72.6	87.0	61.9	46.8
<b>SEA-PRIME</b>	Vicuna-7B	384	81.4	67.2	63.1	73.9	75.6	88.4	63.8	44.2
<b>SEA-PRIME</b>	Llama3-8B	384	<b>83.1</b>	<b>68.0</b>	<b>65.1</b>	79.0	76.0	87.4	<b>64.7</b>	46.0
<b>SEA-PRIME</b>	Vicuna-13B	384	<u>81.9</u>	66.2	64.3	<b>80.9</b>	<b>76.9</b>	86.7	63.6	<b>48.8</b>

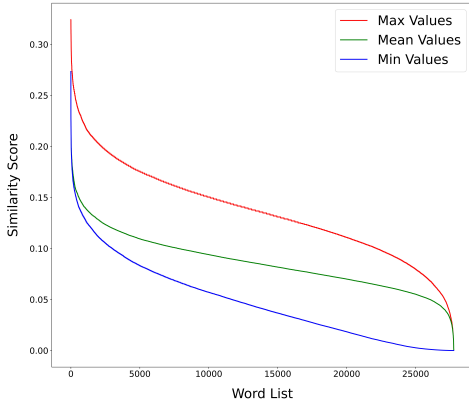
### 5.1 Experimental Setup

**Architecture.** We conducted extensive experiments to evaluate the generalization of SEA across different components of the MLLMs. 1) Vision Encoders. We explored the performance of SEA with three widely-used vision encoders: CLIP-ViT-L@336px [40], SigLIP-ViT-SO@384px [49], and S<sup>2</sup>-Wrapper@1008px [43]. 2) LLMs. To test the scalability of SEA, we applied it to various LLMs with parameters ranging from 2B to 13B. This included Gemma-2B [16], Phi-3-mini-4k-instruct [1], Llama3-8B-Instruct [3] and Vicuna-1.5-7B&13B [11]. 3) SEA Implementation. For SEA, we selected the top 10 labels based on similarity (i.e.,  $n = 10$ ), and set the temperature  $\tau = 0$  to ensure robust alignment. Meanwhile, we perform sampling with a  $2 * 2$  window. This setup allowed us to comprehensively evaluate the effectiveness of SEA in enhancing cross-modal alignment.

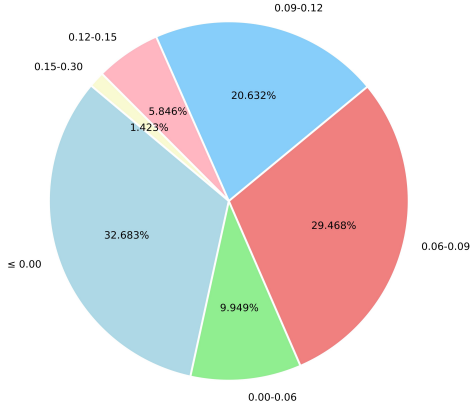
**Training Details.** We perform a two-stage training process. In the first stage, only the adapter was optimized while the vision encoder was fixed. In the second stage, both the LLM and the adapter were optimized. However, for SEA-PRIME, the vision encoder was also tuned during the second stage with a learning rate of  $2e-6$ . Regarding the training scheme, we optimize all the models for 1 epoch with the AdamW optimizer and a cosine learning schedule following LLaVA’s hyperparameters [33]. The training time for models in Table 2 ranges from 6 to 10 hours using  $8 \times H800$  GPUs, which is nearly identical to LLaVA’s training duration, with Stage 1 requiring only an additional 10-20 minutes. For SEA-PRIME, the training time is less than 4 days with the same GPU configuration.



**Datasets.** For our models in Table 1, we use the Cambrian-1 [45] training data, which consists of 2.5M caption pairs for modality alignment and Cambrian-7M data for instruction tuning. All ablation experiments in Table 2 utilize the same data as LLaVA-1.5, specifically the CC-595K dataset [34] for pre-training and a 656K mixture dataset [33], which includes LLaVA-Instruct [34], TextVQA [44], GQA [20], OCR-VQA [37], and Visual Genome [25] for instruction-tuning.



(a) Similarity score of each word.



(b) Distribution of similarity scores.

**Figure 6: Cosine Similarity Analysis of Word List.** Based on cosine similarity scores, we analyzed the semantic labels for each visual patch and the usage patterns of every word in the entire vocabulary. In Figure 6a, we obtained semantic labels for all visual patches using the method below, compiled those with similarity scores greater than 0, and plotted their distribution. In Figure 6b, we depicted the distribution of average similarity scores for each word across the entire vocabulary.

**Word List.** We used the 2of12 word list from the 12 dictionary corpus, containing 41,242 words. The LLaVA-Pretrain dataset was processed following the pipeline shown in Figure 5, assigning relevant semantic labels to each visual patch. After defining the semantic labels as described in Section 4, we set the similarity scores of all other words in the word list to 0. Finally, we analyze the distribution of the similarity scores of the word list (See Figure 6). While many candidate labels show low cosine similarities to their corresponding image patches, a notable peak in the distribution around a higher similarity value of 0.3 suggests a cluster of candidate labels strongly aligned semantically with the image patches. It highlights the set’s rich semantic content and ability to capture diverse and meaningful representations of visual information. As shown in Figure 6b, the similarity scores of semantic labels cluster around 0.08, with about 32.7% of labels having cosine similarities less than 0. Notably, we achieve a utilization rate of 61.2% for the 2of12 word list, suggesting that the 2of12 list offers ample vocabulary to support our semantic labels.

## 5.2 Experimental Results

We leverage the SEA method to train a family of MLLMs called SEA-PRIME. Our models utilize LLM backbones of various scales. The vision component employs SigLIP-ViT-SO400M/14@384. We pre-train the connector using 2.5M adapter data and instruction tune using Cambrian-7M data.

In our evaluations on benchmarks, SEA-PRIME models demonstrate significant improvements over existing open-source methods across various settings, as shown in Table 1. Specifically, our SEA-PRIME models exhibit superior performance with the 2B and 3.8B parameter model compared to the efficient MobileVLM, achieving competitive results despite its smaller scale. The scalability of SEA-PRIME is evident when larger LLMs are employed. Notably, with the LLaMA-3-Instruct-8B, SEA-PRIME achieves exceptional results, showcasing the effectiveness of our approach.

As shown in Figure 1a, LLaVA’s performance is underwhelming due to its unsupervised pre-training, which turns visual tokens into ‘additional vocabulary’. We introduced SEA during pre-training, allowing the adapter to better transform visual representations (See Figure 1b) and providing better initialization weights for instruction tuning. To validate the latter, we evaluated the language model

Table 2: **Exploring the Compatibility and Scalability of SEA.** Scaling results on LLM, vision encoder (VE) and resolution (Res.) are provided. "0.5M+0.6M" denotes the training data from LLaVA-1.5 [33]. Results with SEA are marked in  .

Method	VE	Res.	PT+IT	LLM	VQA <sup>v2</sup>	VQA <sup>T</sup>	GQA	SQA <sup>1</sup>	MMB	POPE	VizWiz	MM-Vet
LLaVA [33]	CLIP-L	336	0.5M+0.6M	Vicuna-7B	78.8	58.3	62.0	67.9	66.2	86.5	45.7	30.7
SEA-LLaVA	CLIP-L	336	0.5M+0.6M	Vicuna-7B	<b>79.1</b>	<b>58.9</b>	<b>63.2</b>	<b>69.4</b>	<b>66.8</b>	<b>87.6</b>	<b>48.8</b>	<b>31.9</b>
<i>Applying to Different LLMs</i>												
LLaVA [33]	CLIP-L	336	0.5M+0.6M	Gemma-2B	72.5	43.7	56.0	61.3	54.0	84.4	38.7	23.9
+ SEA	CLIP-L	336	0.5M+0.6M	Gemma-2B	<b>76.6</b>	<b>49.7</b>	<b>60.9</b>	<b>62.5</b>	<b>59.5</b>	<b>87.0</b>	<b>39.5</b>	<b>27.6</b>
LLaVA [33]	CLIP-L	336	0.5M+0.6M	Phi3-3.8B	77.4	54.6	60.8	73.0	68.7	86.5	37.1	<b>35.4</b>
+ SEA	CLIP-L	336	0.5M+0.6M	Phi3-3.8B	<b>77.5</b>	<b>55.3</b>	<b>61.0</b>	<b>74.2</b>	<b>69.4</b>	<b>87.0</b>	<b>39.0</b>	34.7
LLaVA [33]	CLIP-L	336	0.5M+0.6M	LlaMA3-8B	79.4	57.7	63.7	76.0	<b>72.5</b>	87.0	<b>48.1</b>	34.0
+ SEA	CLIP-L	336	0.5M+0.6M	LlaMA3-8B	<b>79.6</b>	<b>58.0</b>	<b>63.8</b>	<b>76.6</b>	72.0	87.0	45.2	<b>36.3</b>
LLaVA [33]	CLIP-L	336	0.5M+0.6M	Vicuna-13B	<b>80.0</b>	<b>60.8</b>	63.3	71.6	67.7	87.6	53.6	35.1
+ SEA	CLIP-L	336	0.5M+0.6M	Vicuna-13B	79.8	60.4	<b>63.8</b>	<b>71.7</b>	<b>68.0</b>	87.6	<b>57.3</b>	<b>35.8</b>
<i>Scaling to higher resolution</i>												
LLaVA [33]	SigLIP-SO	384	0.5M+0.6M	Vicuna-7B	80.8	62.3	63.2	70.6	68.0	86.7	51.1	32.9
+ SEA	SigLIP-SO	384	0.5M+0.6M	Vicuna-7B	<b>80.9</b>	<b>62.6</b>	<b>63.4</b>	<b>71.3</b>	<b>68.4</b>	<b>87.3</b>	<b>52.4</b>	<b>34.6</b>
S <sup>2</sup> -Wrapper [43]	CLIP-L	1008	0.5M+0.6M	Vicuna-7B	79.7	60.3	63.2	68.3	<b>67.3</b>	87.4	<b>50.7</b>	33.0
+ SEA	CLIP-L	1008	0.5M+0.6M	Vicuna-7B	<b>79.8</b>	<b>60.6</b>	<b>63.7</b>	<b>69.0</b>	66.4	<b>87.5</b>	48.5	<b>33.2</b>

Table 3: **Exploring Ablation for Fine-tuning Vision Encoder.** The baseline is LLaVA-1.5 [33] with Vicuna-7B, using the same training data and strategy. "Finetune VE" refers to the method where the vision encoder is unfrozen during instruction tuning.

Method	VQA <sup>v2</sup>		VQA <sup>T</sup>		GQA		SQA		MMB		VizWiz	
Baseline	78.8		58.3		62.0		67.9		66.2		45.7	
+ <i>Finetune VE</i>	80.3	+1.5 <span style="color: green;">█</span>	59.1	+0.8 <span style="color: green;">█</span>	63.4	+1.4 <span style="color: green;">█</span>	67.0	-0.9 <span style="color: blue;">█</span>	66.1	-0.1 <span style="color: blue;">█</span>	50.3	+4.6 <span style="color: green;">█</span>
+ SEA	<b>80.5</b>	+0.2 <span style="color: green;">█</span>	<b>59.5</b>	+0.4 <span style="color: green;">█</span>	<b>63.6</b>	+0.2 <span style="color: green;">█</span>	<b>69.5</b>	+2.5 <span style="color: green;">█</span>	<b>68.0</b>	+1.9 <span style="color: green;">█</span>	<b>51.6</b>	+1.3 <span style="color: green;">█</span>

using the MMLU benchmark after fine-tuning. As shown in Figure 3, SEA effectively preserves LLM’s language capabilities.

### 5.3 Ablation study

We conducted an extensive ablation study to evaluate the effectiveness of our proposed Supervised Embedding Alignment (SEA). Table 2 showcases the evaluation results across 8 popular benchmarks. These results demonstrate the efficacy of our proposed SEA technique in enhancing the alignment between visual representations and the LLM’s embedding space and significantly outperforming LLaVA-1.5, making it a highly adaptable solution for diverse multimodal integration scenarios.

**Applying to Different LLMs.** Our experiments explore the application of SEA across LLMs of varying sizes, including the Gemma-2B [16], Phi-3-mini-4k-instruct [1], Vicuna-1.5-7B&13B [11], and LlaMA3-8B-Instruct [3]. Notably, for the smaller model, SEA significantly boosts performance across multiple tasks. This highlights SEA’s ability to effectively address misalignment issues that are more pronounced in smaller LLMs, thereby enhancing their performance. Larger LLMs, while inherently better at handling misalignment, still benefit from SEA, indicating that SEA offers additional alignment gains regardless of model size.

**Scaling to Higher Resolution.** We also examined the impact of SEA with different vision encoders. Replacing the CLIP-ViT [40] with the SigLIP-SO(400M) [49], SEA consistently boosts performance, underscoring SEA’s versatility and robustness across different encoder architectures. Using the S<sup>2</sup>-Wrapper [43] at 1008px resolution, SEA again demonstrated its effectiveness by improving performance across the board. These results indicate that higher resolution inputs, which provide more detailed visual information, further enhance SEA’s supervised alignment process.

**Finetune Vision Encoders Based on SEA.** [45] has demonstrated that unfreezing the vision encoder during the fine-tuning stage is always beneficial. We conducted ablation experiments based on Vicuna-1.5-7B [11]. The experimental results, as shown in Table 3, illustrate that alignment training

via SEA, combined with unfreezing the vision encoder during the fine-tuning stage, consistently yields positive benefits across all evaluated benchmarks. Compared to only using either SEA or unfreezing the vision encoder during fine-tuning, the combined approach is a more effective training strategy, indicating that SEA enhances the benefits obtained from unfreezing the vision encoder.

## 6 Conclusion and Discussion

In this paper, we present Supervised Embedding Alignment (SEA), a straightforward and broadly applicable method based on vision-language pre-trained vision encoders in multimodal LLMs. Unlike most prior studies that focused on aligning vision and language representations solely through a customized adapter, our approach explores the novel direction of enhancing alignment with supervision during pre-training to improve the performance of multimodal LLMs. Our experiments demonstrate that SEA leads to significant improvements across multiple benchmarks. Additionally, SEA exhibits robustness and versatility, making it applicable to a variety of vision encoders and large language models. The proposed approach effectively utilizes the strengths of vision-language pre-trained models, potentially unlocking new frontiers in multimodal reasoning capabilities.

However, despite the benefits SEA brings to the performance of Multimodal LLMs, there are notable limitations that need addressing. Firstly, obtaining alignment labels in SEA constrains its applicability, as it currently relies on pre-trained vision encoders aligned with vision-language pairs. Extending SEA to effectively align and supervise autoregressive vision encoders [10, 19, 38] or other types of vision encoders [23, 41] remains an area for further research. Moreover, finding an optimal representation for each visual token in the embedding space remains a significant challenge, impacting how LLMs interpret these tokens. There is also concern that manually guiding the adapter for semantic alignment might result in the loss of additional information in the visual tokens. Addressing these issues requires the development of more effective alignment methods, which will be crucial for further enhancing the capabilities and robustness of multimodal LLMs.

## References

- [1] M. Abdin, S. A. Jacobs, A. A. Awan, J. Aneja, A. Awadallah, H. Awadalla, N. Bach, A. Bahree, A. Bakhtiari, J. Bao, H. Behl, et al. Phi-3 technical report: A highly capable language model locally on your phone, 2024.
- [2] H. Agrawal, K. Desai, Y. Wang, X. Chen, R. Jain, M. Johnson, D. Batra, D. Parikh, S. Lee, and P. Anderson. Nocaps: Novel object captioning at scale. In *Proceedings of the IEEE/CVF international conference on computer vision*, pages 8948–8957, 2019.
- [3] AI@Meta. Llama 3 model card. 2024.
- [4] J.-B. Alayrac, J. Donahue, P. Luc, A. Miech, I. Barr, Y. Hasson, K. Lenc, A. Mensch, K. Millican, M. Reynolds, et al. Flamingo: a visual language model for few-shot learning. In *NeurIPS*, 2022.
- [5] S. Antol, A. Agrawal, J. Lu, M. Mitchell, D. Batra, C. L. Zitnick, and D. Parikh. VQA: Visual question answering. In *IEEE ICCV*, pages 2425–2433, 2015.
- [6] A. Awadalla, I. Gao, J. Gardner, J. Hessel, Y. Hanafy, W. Zhu, K. Marathe, Y. Bitton, S. Gadre, S. Sagawa, et al. Openflamingo: An open-source framework for training large autoregressive vision-language models. *arXiv preprint arXiv:2308.01390*, 2023.
- [7] J. Bai, S. Bai, S. Yang, S. Wang, S. Tan, P. Wang, J. Lin, C. Zhou, and J. Zhou. Qwen-vl: A frontier large vision-language model with versatile abilities. *arXiv preprint arXiv:2308.12966*, 2023.
- [8] I. Bica, A. Ilić, M. Bauer, G. Erdogan, M. Bošnjak, C. Kaplanis, A. A. Gritsenko, M. Minderer, C. Blundell, R. Pascanu, and J. Mitrović. Improving fine-grained understanding in image-text pre-training, 2024.
- [9] L. Chen, J. Li, X. Dong, P. Zhang, C. He, J. Wang, F. Zhao, and D. Lin. Sharegpt4v: Improving large multi-modal models with better captions, 2023.

- [10] X. Chen, S. Xie, and K. He. An empirical study of training self-supervised vision transformers. In *Proceedings of the IEEE/CVF international conference on computer vision*, pages 9640–9649, 2021.
- [11] W.-L. Chiang, Z. Li, Z. Lin, Y. Sheng, Z. Wu, H. Zhang, L. Zheng, S. Zhuang, Y. Zhuang, J. E. Gonzalez, I. Stoica, and E. P. Xing. Vicuna: An open-source chatbot impressing gpt-4 with 90%\* chatgpt quality. <https://lmsys.org/blog/2023-03-30-vicuna/>, 2023.
- [12] X. Chu, L. Qiao, X. Lin, S. Xu, Y. Yang, Y. Hu, F. Wei, X. Zhang, B. Zhang, X. Wei, and C. Shen. Mobilevlm : A fast, strong and open vision language assistant for mobile devices, 2023.
- [13] X. Chu, L. Qiao, X. Zhang, S. Xu, F. Wei, Y. Yang, X. Sun, Y. Hu, X. Lin, B. Zhang, and C. Shen. Mobilevlm v2: Faster and stronger baseline for vision language model, 2024.
- [14] W. Dai, J. Li, D. Li, A. M. H. Tiong, J. Zhao, W. Wang, B. Li, P. Fung, and S. Hoi. Instructblip: Towards general-purpose vision-language models with instruction tuning. *arXiv:2305.06500*, 2023.
- [15] D. Driess, F. Xia, M. S. M. Sajjadi, C. Lynch, A. Chowdhery, B. Ichter, A. Wahid, J. Tompson, Q. Vuong, T. Yu, W. Huang, Y. Chebotar, P. Sermanet, D. Duckworth, S. Levine, V. Vanhoucke, K. Hausman, M. Toussaint, K. Greff, A. Zeng, I. Mordatch, and P. Florence. Palm-e: an embodied multimodal language model. In *Proceedings of the 40th International Conference on Machine Learning, ICML’23*. JMLR.org, 2023.
- [16] Google. Gemma: Introducing new state-of-the-art open models. <https://blog.google/technology/developers/gemma-open-models/>, 2024.
- [17] Y. Goyal, T. Khot, D. Summers-Stay, D. Batra, and D. Parikh. Making the v in vqa matter: Elevating the role of image understanding in visual question answering. In *CVPR*, 2017.
- [18] D. Gurari, Q. Li, A. J. Stangl, A. Guo, C. Lin, K. Grauman, J. Luo, and J. P. Bigham. Vizwiz grand challenge: Answering visual questions from blind people, 2018.
- [19] K. He, X. Chen, S. Xie, Y. Li, P. Dollár, and R. Girshick. Masked autoencoders are scalable vision learners. In *Proceedings of the IEEE/CVF conference on computer vision and pattern recognition*, pages 16000–16009, 2022.
- [20] D. A. Hudson and C. D. Manning. GQA: A new dataset for real-world visual reasoning and compositional question answering. In *IEEE CVPR*, pages 6700–6709, 2019.
- [21] C. Jia, Y. Yang, Y. Xia, Y.-T. Chen, Z. Parekh, H. Pham, Q. Le, Y.-H. Sung, Z. Li, and T. Duerig. Scaling up visual and vision-language representation learning with noisy text supervision. In *ICML*, 2021.
- [22] A. Q. Jiang, A. Sablayrolles, A. Mensch, C. Bamford, D. S. Chaplot, D. de las Casas, F. Bressand, G. Lengyel, G. Lample, L. Saulnier, L. R. Lavaud, M.-A. Lachaux, P. Stock, T. L. Scao, T. Lavril, T. Wang, T. Lacroix, and W. E. Sayed. Mistral 7b, 2023.
- [23] A. Kirillov, E. Mintun, N. Ravi, H. Mao, C. Rolland, L. Gustafson, T. Xiao, S. Whitehead, A. C. Berg, W.-Y. Lo, et al. Segment anything. In *Proceedings of the IEEE/CVF International Conference on Computer Vision*, pages 4015–4026, 2023.
- [24] J. Y. Koh, R. Salakhutdinov, and D. Fried. Grounding language models to images for multimodal inputs and outputs, 2023.
- [25] R. Krishna, Y. Zhu, O. Groth, J. Johnson, K. Hata, J. Kravitz, S. Chen, Y. Kalantidis, L.-J. Li, D. A. Shamma, et al. Visual Genome: Connecting language and vision using crowdsourced dense image annotations. *IJCV*, 123:32–73, 2017.
- [26] H. Laurençon, L. Saulnier, L. Tronchon, S. Bekman, A. Singh, A. Lozhkov, T. Wang, S. Karamcheti, A. M. Rush, D. Kiela, M. Cord, and V. Sanh. OBELICS: An open web-scale filtered dataset of interleaved image-text documents. In *Thirty-seventh Conference on Neural Information Processing Systems Datasets and Benchmarks Track*, 2023.

- [27] J. Li, D. Li, S. Savarese, and S. Hoi. Blip-2: Bootstrapping language-image pre-training with frozen image encoders and large language models. *arXiv:2301.12597*, 2023.
- [28] Y. Li, Y. Du, K. Zhou, J. Wang, W. X. Zhao, and J.-R. Wen. Evaluating object hallucination in large vision-language models. *arXiv preprint arXiv:2305.10355*, 2023.
- [29] Y. Li, C. Wang, and J. Jia. Llama-vid: An image is worth 2 tokens in large language models. *arXiv:2311.17043*, 2023.
- [30] Y. Li, H. Wang, Y. Duan, and X. Li. Clip surgery for better explainability with enhancement in open-vocabulary tasks, 2023.
- [31] Y. Li, Y. Zhang, C. Wang, Z. Zhong, Y. Chen, R. Chu, S. Liu, and J. Jia. Mini-gemini: Mining the potential of multi-modality vision language models, 2024.
- [32] Y. Lin, Y. Li, D. Chen, W. Xu, R. Clark, P. Torr, and L. Yuan. Rethinking visual prompting for multimodal large language models with external knowledge. *arXiv preprint arXiv:2407.04681*, 2024.
- [33] H. Liu, C. Li, Y. Li, and Y. J. Lee. Improved baselines with visual instruction tuning. *arXiv preprint arXiv:2310.03744*, 2023.
- [34] H. Liu, C. Li, Q. Wu, and Y. J. Lee. Visual instruction tuning. *NeurIPS*, 36, 2024.
- [35] Y. Liu, H. Duan, Y. Zhang, B. Li, S. Zhang, W. Zhao, Y. Yuan, J. Wang, C. He, Z. Liu, et al. MMBench: Is your multi-modal model an all-around player? *arXiv preprint arXiv:2307.06281*, 2023.
- [36] P. Lu, S. Mishra, T. Xia, L. Qiu, K.-W. Chang, S.-C. Zhu, O. Tafjord, P. Clark, and A. Kalyan. Learn to explain: Multimodal reasoning via thought chains for science question answering. *Advances in Neural Information Processing Systems*, 35:2507–2521, 2022.
- [37] A. Mishra, S. Shekhar, A. K. Singh, and A. Chakraborty. OCR-VQA: Visual question answering by reading text in images. In *IEEE ICDAR*, pages 947–952, 2019.
- [38] M. Oquab, T. Darcet, T. Moutakanni, H. Vo, M. Szafraniec, V. Khalidov, P. Fernandez, D. Haziza, F. Massa, A. El-Nouby, et al. Dinov2: Learning robust visual features without supervision. *arXiv preprint arXiv:2304.07193*, 2023.
- [39] J. Park, J. Lee, and K. Sohn. Bridging vision and language spaces with assignment prediction. *arXiv preprint arXiv:2404.09632*, 2024.
- [40] A. Radford, J. W. Kim, C. Hallacy, A. Ramesh, G. Goh, S. Agarwal, G. Sastry, A. Askell, P. Mishkin, J. Clark, et al. Learning transferable visual models from natural language supervision. In *ICML*, 2021.
- [41] R. Rombach, A. Blattmann, D. Lorenz, P. Esser, and B. Ommer. High-resolution image synthesis with latent diffusion models. In *Proceedings of the IEEE/CVF conference on computer vision and pattern recognition*, pages 10684–10695, 2022.
- [42] Y. Shang, M. Cai, B. Xu, Y. J. Lee, and Y. Yan. Llava-prumerge: Adaptive token reduction for efficient large multimodal models. *arXiv preprint arXiv:2403.15388*, 2024.
- [43] B. Shi, Z. Wu, M. Mao, X. Wang, and T. Darrell. When do we not need larger vision models?, 2024.
- [44] A. Singh, V. Natarajan, M. Shah, Y. Jiang, X. Chen, D. Batra, D. Parikh, and M. Rohrbach. Towards vqa models that can read. In *CVPR*, 2019.
- [45] S. Tong, E. Brown, P. Wu, S. Woo, M. Middepogu, S. C. Akula, J. Yang, S. Yang, A. Iyer, X. Pan, A. Wang, R. Fergus, Y. LeCun, and S. Xie. Cambrian-1: A fully open, vision-centric exploration of multimodal llms, 2024.
- [46] W. Wang, Q. Lv, W. Yu, W. Hong, J. Qi, Y. Wang, J. Ji, Z. Yang, L. Zhao, X. Song, et al. Cogvlm: Visual expert for pretrained language models. *arXiv:2311.03079*, 2023.

- [47] A. Yan, Z. Yang, J. Wu, W. Zhu, J. Yang, L. Li, K. Lin, J. Wang, J. McAuley, J. Gao, and L. Wang. List items one by one: A new data source and learning paradigm for multimodal llms, 2024.
- [48] W. Yu, Z. Yang, L. Li, J. Wang, K. Lin, Z. Liu, X. Wang, and L. Wang. Mm-vet: Evaluating large multimodal models for integrated capabilities, 2023.
- [49] X. Zhai, B. Mustafa, A. Kolesnikov, and L. Beyler. Sigmoid loss for language image pre-training, 2023.
- [50] F. Zhao, T. Pang, C. Li, Z. Wu, J. Guo, S. Xing, and X. Dai. Aligngpt: Multi-modal large language models with adaptive alignment capability. *arXiv preprint arXiv:2405.14129*, 2024.
- [51] B. Zhou, Y. Hu, X. Weng, J. Jia, J. Luo, X. Liu, J. Wu, and L. Huang. Tinyllava: A framework of small-scale large multimodal models, 2024.
- [52] D. Zhu, J. Chen, X. Shen, X. Li, and M. Elhoseiny. Minigpt-4: Enhancing vision-language understanding with advanced large language models. *arXiv:2304.10592*, 2023.
- [53] Y. Zhu, M. Zhu, N. Liu, Z. Ou, X. Mou, and J. Tang. Llava-phi: Efficient multi-modal assistant with small language model, 2024.